Bioinformatics, 38(7), 2022, 1895–1903
https://doi.org/10.1093/bioinformatics/btac056
Advance Access Publication Date: 3 February 2022
Original Paper

Structural bioinformatics

DeepUMQA: ultrafast shape recognition-based protein model quality assessment using deep learning

Sai-Sai Guo†, Jun Liu†, Xiao-Gen Zhou and Gui-Jun Zhang *

College of Information Engineering, Zhejiang University of Technology, Hangzhou 310023, China

*To whom correspondence should be addressed.
†The authors wish it to be known that, in their opinion, the first two authors should be regarded as Joint First Authors.

Associate Editor: Lenore Cowen

Received on October 2, 2021; revised on December 26, 2021; editorial decision on January 23, 2022; accepted on January 27, 2022

Abstract

Motivation: Protein model quality assessment is a key component of protein structure prediction. In recent research, the voxelization feature was used to characterize the local structural information of residues, but it may be insufficient for describing residue-level topological information. Design features that can further reflect residue-level topology when combined with deep learning methods are therefore crucial to improve the performance of model quality assessment.

Results: We developed a deep-learning method, DeepUMQA, based on Ultrafast Shape Recognition (USR) for the residue-level single-model quality assessment. In the framework of the deep residual neural network, the residue-level USR feature was introduced to describe the topological relationship between the residue and overall structure by calculating the first moment of a set of residue distance sets and then combined with 1D, 2D and voxelization features to assess the quality of the model. Experimental results on the CASP13, CASP14 test datasets and CAMEO blind test show that USR could supplement the voxelization features to comprehensively characterize residue structure information and significantly improve model assessment accuracy. The performance of DeepUMQA ranks among the top during the state-of-the-art single-model quality assessment methods, including ProQ2, ProQ3, ProQ3D, Ornate, VoroMQA, ProteinGCN, ResNetQA, QDeep, GraphQA, ModFOLD6, ModFOLD7, ModFOLD8, QMEAN3, QMEANDisCo3 and DeepAccNet.

Availability and implementation: The DeepUMQA server is freely available at http://zhanglab-bioinf.com/DeepUMQA/.

Contact: zgj@zjut.edu.cn

Supplementary information: Supplementary data are available at *Bioinformatics* online.

1 Introduction

Proteins are the basis of life matter and ubiquitous in almost all biological processes. High-throughput acquisition of the protein structure helps in understanding its function and mechanism of action (Senior *et al.*, 2020; Yang *et al.*, 2015; Zhou *et al.*, 2019a). Although the current sequencing technology can quickly and cheaply determine the primary sequence of a protein, determining the 3D structure of a protein is still difficult and expensive (Zhang *et al.*, 2017; Zhou *et al.*, 2019b). In the past few decades, many methods have been proposed to predict the 3D structure of a protein directly from the primary sequence (Leaver-Fay *et al.*, 2011; Liu *et al.*, 2020, 2021; Moult *et al.*, 2018; Rohl *et al.*, 2004; Xu and Zhang, 2012; Zheng *et al.*, 2021). In particular, the introduction of *deep* residual neural networks has promoted the rapid development of structural prediction (AlQuraishi, 2019; Kryshtafovych *et al.*, 2019; Kuhlman and Bradley, 2019; Mao *et al.*, 2020; Wang *et al.*, 2017; Xu *et al.*, 2019; Yang *et al.*, 2020). In CASP14, the predicted model of AlphaFold2 in most target proteins is comparable with that of experimental structures (Jumper *et al.*, 2021). Assessing the quality of the generated protein model is a fundamental part of protein structure prediction, which is important for further structure refinement and reliable identification of the best models (Cheng *et al.*, 2019; Shuvo *et al.*, 2020).

In general, protein model assessment methods can be divided into two categories. The first covers single-model quality assessment approaches, which take a single structural model as an input, extract features that can reflect model information, and use machine learning methods to infer the quality of the model (Hiranuma *et al.*, 2021; Jing and Xu, 2021; Olechnovic and Venclovas, 2017; Pagès *et al.*, 2019; Ray *et al.*, 2012; Uziela *et al.*, 2016). The second one encompasses consensus methods, which evaluate protein models by using information from other models in a pool of candidate models (Cheng *et al.*, 2009; Ginalski *et al.*, 2003; Lundström *et al.*, 2001). Although consensus methods achieve high correlations between predicted and true quality measures, their performance is greatly

affected by the size and diversity of the input model pool (Cao *et al.*, 2017). When the models lack consensus or are similar, the consensus method cannot easily select the best model (Shuvo *et al.*, 2020). By contrast, single-model quality assessment methods are not limited by the model pool and can independently score and select models. Single-model quality assessment methods have elicited increasing attention in the recent Critical Assessment of Techniques for Protein Structure Prediction (CASP) (Cheng *et al.*, 2019; Kryshtafovych *et al.*, 2018; Manavalan *et al.*, 2017; McGuffin *et al.*, 2019). In CASP14, single-model quality assessment methods account for more than 70% of all model quality assessment methods (Kwon *et al.*, 2021).

Single-model quality assessment methods usually use different feature combinations and machine learning methods to learn the implicit relationship between a model's structure and its quality. ProQ2 predicts the local and global quality of protein models by using support vector machine (SVM) and weighting the sequence spectra of residue specific features including atom-atom contacts, residue–residue contacts and surface area, predicted and observed secondary structures (Ray *et al.*, 2012). ProQ3 uses Rosetta energy terms, which are based on the full-atom model and simplified centroid side chain representation (centroid model), as input features to train the same SVM employed in ProQ2 (Uziela *et al.*, 2016). VoroMQA combines the idea of statistical potentials with the use of interatomic contact area, which is adopted to describe and seamlessly integrate explicit interactions between protein atoms and implicit interactions of protein atoms with the solvent (Olechnovic and Venclovas, 2017). With the introduction of the convolutional residual neural network (ResNet) into protein structure prediction, an increasing number of single-model quality assessment methods utilize deep learning (Xu and Wang, 2019). ProQ3D replaces SVM in ProQ3 with multilayer perceptron, which significantly improves the accuracy of model assessment (Uziela *et al.*, 2017). Ornate predicts local (residue-wise) and global model quality based on 3D voxel atomic representation and 3D convolutional network. The input density map corresponding to each residue and its neighborhood is aligned with the backbone topology of this residue as the voxelization feature of residues that are translationally and rotationally invariant (Pagès *et al.*, 2019). DeepAccNet uses 3D and 2D convolution to predict the per-residue accuracy and residue–residue distance signed error in protein models and employs these predictions to guide Rosetta protein structure refinement, in which 3D convolution similar to that in Ornate is used to evaluate the local atomic environment, and 2D convolution is adopted to provide the global context (Hiranuma *et al.*, 2021). ProteinGCN represents the initial model as a graph, in which atoms, residues, and geometric features are first extracted; then, a graph neural network (GNN) is subsequently used to predict the quality of the protein model (Sanyal *et al.*, 2020). GNNRefine applies GNN to predict the refined inter-atom distance probability distribution of the input model for further protein model refinement (Jing and Xu, 2021). Existing methods show that feature extraction and network model training are important for model quality assessment, and designing appropriate features helps infer the implicit relationship between model structure and its quality.

In this work, we developed an Ultrafast Shape Recognition (USR)-based residue-level single model quality assessment method, termed DeepUMQA. The residue-level USR feature is used to map the topological information of the model to each residue, thereby characterizing the relationship between the residue and the topological structure (i.e. the topological information of the residue), which is combined with the residue voxelization feature (i.e. the local structure information of the residue), secondary structure, distances and Rosetta energy terms, and use three-dimensional convolution, two-dimensional convolution and residual networks to predict the quality of the protein model. Experimental results show that the USR feature is complementary to the voxelization feature in describing residues from local and topological aspects, and it can thus significantly improve the performance of model quality assessment.

2 Materials and methods

The pipeline of DeepUMQA is shown in Figure 1. It consists of four steps, namely, data preparation, feature extraction, network architecture and model training and lDDT calculation for model quality assessment.

2.1 Data preparation

We construct a non-redundant protein dataset from the PISCES server (deposited by May, 2018) (Wang *et al.*, 2003), and the filter criteria are set as follows: (i) maximum sequence redundancy of 40%, (ii) minimum resolution of 2.5 Å, (iii) each protein chain is limited to 50–300 residues and (iv) the protein be either a monomer or interact with other chains with minimum (less than 1 kcal/mol of Rosetta energy). The dataset contains 7615 proteins (7226 for training and 389 for validation). Four methods including Rosetta stochastic modeling (Rohl *et al.*, 2004), comparative modeling from RosettaCM (Song *et al.*, 2013), native structure perturbation and folding guided by the deep learning method trRosetta (Yang *et al.*, 2020) are used to generate structure models with variety and a reasonable precision distribution. Each protein generates about 150 decoys, and each decoy is relaxed through Rosetta dual-relax (Conway *et al.*, 2014 Gabriel, 2020). To test the performance of DeepUMQA, we collect a test dataset consisting of 51 CASP13, 44 CASP14 targets that is strictly non-redundant with the training set (sequence redundancy below 30%). In addition, we have participated in the blind test of CAMEO-QE for one month (November 26, 2021 to December 18,

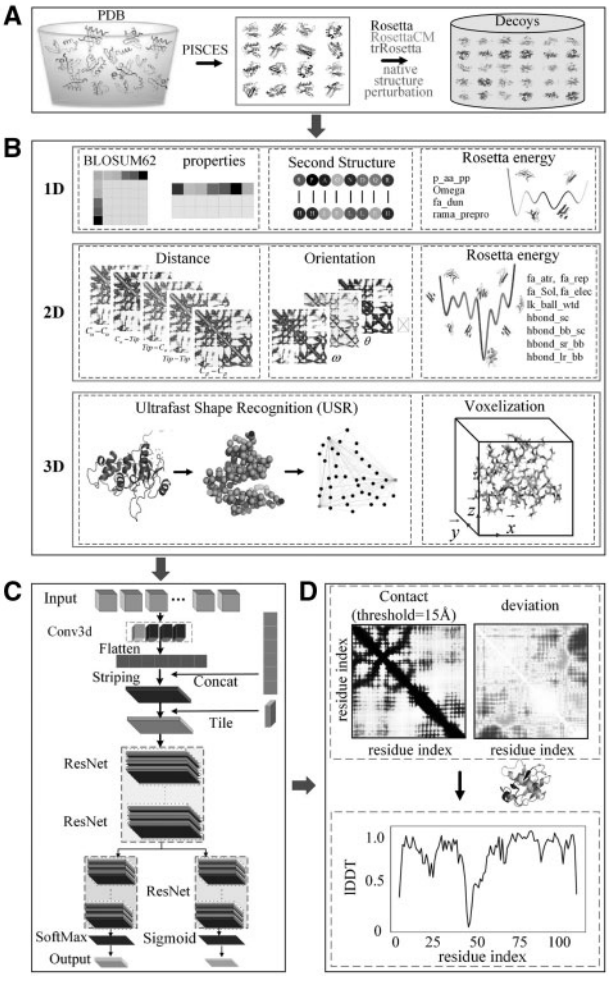

Fig. 1. Pipeline of DeepUMQA. (**A**) Data preparation. (**B**) Feature extraction. (**C**) Network architecture. (**D**) Model training and lDDT calculation

2021), which included 54 targets. The detailed information of these targets are listed in Supplementary Tables S5–S7 in Supplementary Material. Each target of CASP13 and CASP14 obtains about 150 models from the official website (https://predictioncenter.org/download_area/), and we submitted the evaluation results of 423 models in the one-month blind test of CAMEO-QE (https://www.cameo3d.org/quality-estimation/), thereby forming a dataset containing 14 486 models in total.

2.2 Features extraction

As shown in Figure 1B, D features (i.e. amino acid sequence properties, secondary structure and Rosetta intra-residue energy terms), 2D features (i.e. residue–residue distance and orientation and Rosetta inter-residue energy terms) and 3D features (i.e. USR and voxelization at the residue level) are extracted for the input model structure. All features are listed in Supplementary Table S1 in Supplementary Material.

2.2.1 Ultrafast Shape Recognition (USR)

Although the Cartesian coordinates of all atoms can completely describe the structural information of the protein model, this representation changes with rotation, which greatly increases the complexity of network training and usage (Hiranuma *et al.*, 2021). To describe the local structure information of residues, previous methods, such as Ornate (Pagès *et al.*, 2019) and DeepAccNet (Hiranuma *et al.*, 2021), voxelize each residue individually in the corresponding local coordinate frame defined by the backbone C, C_α and N atoms. Such representation is translationally and rotationally invariant because projections onto local frames are independent of the global position of the protein structure in 3D space. The voxelization method effectively describes the local structure information of the residue, but it does not fully reflect the topological relationship between the residue and the overall structure. Moreover, the calculation of the voxelization feature vector and 3D convolution are extremely complicated and time consuming.

Inspired by the USR method (Ballester and Richards, 2007; Hao *et al.*, 2016), the topological information of the protein structure can be quickly captured with almost no additional computational cost by selecting an appropriate set of interatomic distances. In particular, this subset can be selected as the set of all atom distances from a reduced number of strategic reference locations. Four reference locations that effectively represent the center and boundary of the protein structure are considered, and a subset of distances between them is utilized to quickly identify the topology of the protein.

In this work, we introduce USR to the residue level to describe the topological relationship between the residues and the overall structure. For a given protein structure model, we extract the USR features of each residue. As shown in Figure 2, for the ith residue, with the current residue r_i as a reference, the residue b_i farthest from the residue r_i and the residue g_i farthest from the residue b_i are determined successively. The topological relationship between the current residue and the overall structure can be described by the three residue distance sets defined by r_i, b_i, g_i. For residue r_i, distances from it to all other residues in the structure are calculated to form a distance set. For residues b_i and g_i, the same method is applied to obtain the corresponding distance set. The distance between residues is calculated according to the distance between the C_β (C_α for glycine) atoms of the residues. The first moment $[\mu_i^r, \mu_i^b, \mu_i^g]$ of the residue distance sets is calculated as the feature mapping of the current residue topology information, and μ_i^r, μ_i^b and μ_i^g are defined as follows:

$$\begin{cases} \mu_i^r = \frac{1}{L}\sum_{i=1}^{L} ||\vec{a_i} - \vec{r_i}||_2 \\ \mu_i^b = \frac{1}{L}\sum_{i=1}^{L} ||\vec{a_i} - \vec{b_i}||_2 \\ \mu_i^g = \frac{1}{L}\sum_{i=1}^{L} ||\vec{a_i} - \vec{g_i}||_2 \end{cases} \quad (1)$$

where L is the sequence length of the protein, $\vec{a_i}$ is the coordinate of the C_β (C_α for glycine) atom of the ith residue, and $\vec{r_i}$, $\vec{b_i}$ and $\vec{g_i}$ are the coordinates of the C_β (C_α for glycine) atoms of the residues r_i, b_i and g_i, respectively.

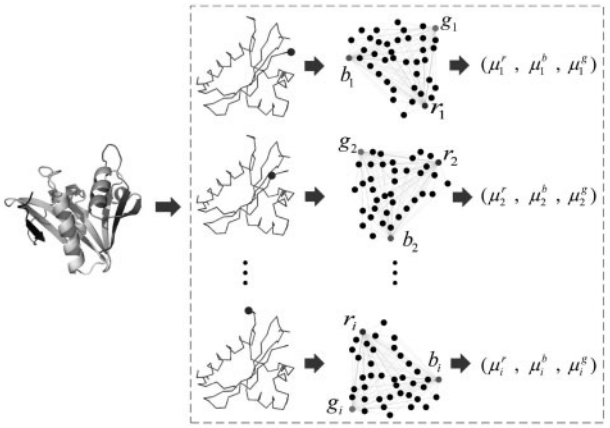

Fig. 2. Residue level USR feature of protein structure. μ_i^r, μ_i^b, μ_i^g are the results of the first moment calculation of the distance sets at the three reference positions: the current residue r_i as a reference, the residue b_i farthest from the residue r_i and the residue g_i farthest from the residue b_i

2.2.2 Amino acid sequence properties and secondary structure

The amino acid sequence contains the 3D structure information of the protein, thus, the properties of the amino acid sequence are important for inferring the quality of the structure model. Blosum62 is a kind of amino acid substitution scoring matrix commonly used in sequence comparison in bioinformatics at present (Henikoff and Henikoff, 1992). It is used to derive the replacement vector of the residue at each position of the structure, thus obtaining an input feature. In addition, we also obtain per amino-acid feature sets from Meiler as the features of individual residues (Meiler *et al.*, 2001). The secondary structure information is also useful for describing the structure of proteins. The DSSP is utilized to obtain the secondary structure characteristic information of the subsequence of the protein structure (Kabsch and Sander, 1983). These feature items are quantified before being used. The per amino acid feature sets from Meiler and Blosum62 scoring matrix are listed in Supplementary Tables S2 and S4 in Supplementary Material, respectively.

2.2.3 Rosetta energy terms

In this work, 13 Rosetta centroid energy terms are also applied as features (Leaver-Fay *et al.*, 2011; Rohl *et al.*, 2004), including one-body-terms (omega, p_aa_pp, fa_dun and rama_prepro), two-body-terms (fa_atr, fa_rep, fa_sol, lk_ball_wtd, fa_elec, hbond_bb_sc and hbond_sc) and the presence of backbone-to-backbone hydrogen bonds (hbond_sr_bb and hbond_lr_bb). The energy terms are normalized before inputting into the deep learning neural network.

2.2.4 Multi-distance and orientations

To effectively describe the information of the protein structure, we use (i) inter-residue C_β distance map, (ii) C_α to tip atom distance map, (iii) tip atom to C_α distance map, (iv) tip atom to tip atom distance map, (v) sequence separation map and (vi) inter-residue orientations (φ, θ, ω) defined by trRosetta (Yang *et al.*, 2020). The sequence separation can be calculated as follows:

$$S_{i,j} = \frac{|i-j|}{\delta - 1} \quad (2)$$

where i and j represent the residue index in the protein sequence and δ represents the normalizer, which is set to 100. The definition of inter-residue orientations can be found in Supplementary Figure S1 in Supplementary Material, and the tip atoms of each residue are listed in Supplementary Table S3 in Supplementary Material.

2.3 Network architecture

For the model architecture side, a typical CNN design starts with a convolutional layer, which processes the high-dimensionality of the input spatial structure data, and then performs a fully connected layer after the dimensionality of the data is reduced. In our design, the 3D convolutional layer learns advanced features, while gradually roughening it and reducing the dimensionality of the data. Then, a set of fully connected layers combine these features and output predictions. Figure 1C shows an overview of the network architecture. First, the 3D voxelization feature passes through a series of 3D convolution layers. The output tensor of 3D convolution layers is flattened into a 1D vector and concatenated with 1D features then goes through a 1D convolution layer. The output tensor of 1D convolution layer is transformed into a 2D tensor by horizontal and vertical striping then combined with other 2D tensor form feature maps. Second, the feature maps are input to a 2D convolutional layer and apply instance normalization. ELU activation is then used. The output is upsampled to 128 channels for the following ResNet operations in this work.

The ResNet operations contains trunk and arm residual blocks. The trunk part consists of 15 residual blocks, each of which is composed of three ELU activation layers, three 2D convolutional layers (dilation is applied with a cycling dilation size of 1, 2, 4, 8 and 16) and three instance normalization layers. The network then branches to two arms of four residual blocks. The output layer distribution of the two arms consists of sigmod and softmax functions to predict C_β distance deviations for all residue pairs (referred to as deviation) and contact map with thresholded at 15 Å. As shown in Supplementary Figure S2 in Supplementary Material, in each residual block, a 'skip-connection' is made between the input and the output layers by skipping the intermediate layer. This connection works as an identity mapping, and its outputs are added to the output of all the layers that were previously stacked and passed to the activation phase of the last layer of the residual block.

2.4 Model training and lDDT calculation

lDDT is a superposition-free score that evaluates the local distance differences of all atoms in a protein structure, and it is well suited for assessing local protein model quality (Mariani *et al.*, 2013). The deviation and contact map thresholded at 15 Å predicted by our deep residual network can be used to calculate the lDDT score of each residue in a protein model. The lDDT score of the ith residue and the global lDDT score are defined as follows:

$$\mathrm{lDDT}_i = \frac{4p_1 + 3p_2 + 2p_3 + p_4}{4p_0} \tag{3}$$

$$\mathrm{lDDT}_{\mathrm{global}} = \frac{1}{L}\sum_{i=1}^{L} lDDT_i \tag{4}$$

where p_0 is the probability that the distance between the ith residue and other residues is within 15 Å, and p_1 is the probability that the absolute value of C_β distance deviation of all the residue pairs whose distance from the ith residue within 15 Å is less than 0.5 Å. In the same manner, p_2, p_3 and p_4 are the probability that the absolute value of C_β distance deviation in all the residue pairs whose distance from the ith residue is within 15 Å is 0.5–1.0 Å, 1.0–2.0 Å and 2.0–4.0 Å, respectively.

The weights in the network are initialized through Xavier initialization (Glorot and Bengio, 2010) with weights drawn from the uniform distribution, and then obtained with the Adam method which is widely used by the neural network model (Jing and Xu, 2021; Kingma and Ba, 2014; Li *et al.*, 2021; Zhou *et al.*, 2020) at an initial learning rate of 0.0005. The multivariate cross-entropy loss function is used to evaluate the residual pair distance deviation loss, and the binary cross-entropy loss function is adopted to evaluate the loss of the contact map with distance cutoff of 15 Å. The mean square loss function is used to evaluate the lDDT loss of each residue. Then, the combination of distance error loss, mask loss and lDDT loss is minimized as:

$$\mathrm{loss} = w_1\mathrm{loss}_{\mathrm{dev}} + w_2\mathrm{loss}_{\mathrm{con}} + w_3\mathrm{loss}_{\mathrm{lDDT}} \tag{5}$$

where $\mathrm{loss}_{\mathrm{dev}}$ is the distance deviation loss, $\mathrm{loss}_{\mathrm{con}}$ is the contact (thresholded at 15 Å) loss, and $\mathrm{loss}_{\mathrm{lDDT}}$ is the lDDT loss of each residue. The weights of each loss w_1, w_2 and w_3 are 1, 1 and 10, respectively.

3 Results and discussion

Global and local evaluation metrics are used to evaluate the performance of model quality assessment. For global evaluation metrics (Global QA), average Pearson and Spearman correlation coefficient, 'top 1 loss' and the area under the ROC curve(AUC) are used (Metz *et al.*, 1978). The average Pearson and Spearman correlation coefficient are used to show the correlation of between the predicted and real global score of protein models, and the higher the correlation, the better the performance (Bolboaca *et al.*, 2006). The 'top 1 loss' is measured by using the lDDT difference between the best model selected based on the predicted lDDT and the actual best model of the target protein, which is used to show the capability to find the best model. The lower the 'top 1 loss', the better the performance (Won *et al.*, 2019). The AUC is used to show the ability to distinguish between good and poor models (or residues), which is measured by the area under the receiver operating characteristic (ROC) curve with an lDDT cutoff value of 0.6 (Ling *et al.*, 2003). For local evaluation metrics (Local QA), per-model Average Pearson and Spearman correlation coefficient, ASE (Average residue-wise S-score error) and AUC were used. The role of Pearson, Spearman correlation coefficient and AUC are the same as global evaluation, the difference is that they are calculated on the local score. ASE measures the average residue-wise S-score error, and the higher the ASE, the better the performance (Kwon *et al.*, 2021).

3.1 Results of CASP targets

The performance of DeepUMQA is tested on 14063 structure models composed of 51 CASP13 and 44 CASP14 targets and compared with the performance of state-of-the-art single-model quality assessment methods, namely, ProQ2 (Ray *et al.*, 2012), ProQ3 (Uziela *et al.*, 2016), ProQ3D (Uziela *et al.*, 2017), VoroMQA (Olechnovic and Venclovas, 2017), Ornate (Pagès *et al.*, 2019), ProteinGCN (Sanyal *et al.*, 2020), ModFOLD7 (Maghrabi and McGuffin, 2020), ModFOLD8 (McGuffin *et al.*, 2021), QDeep (Shuvo *et al.*, 2020), ResNetQA (Jing and Xu, 2020), GraphQA (Baldassarre *et al.*, 2021) and DeepAccNet (Hiranuma *et al.*, 2021). The results of DeepAccNet, ProteinGCN, ResNetQA are obtained by running the official source code locally, and the results of the other methods are obtained from the data archive on the official CASP website (https://predictioncenter.org/download_area/). The performance of DeepUMQA and the comparison methods on the CASP13 and CASP14 datasets are shown in Tables 1 and 2.

For Global QA, the 'top 1 loss' of DeepUMQA is 0.046, which is better than the value of all the comparison methods and Pearson and Spearman correlations of DeepUMQA are 0.834 and 0804, respectively, second only to ModFOLD7 (0.848 and 0.824, respectively) in the CASP13 dataset. In the CASP14 dataset, the Pearson, Spearman correlation and the 'top 1 loss' of DeepUMQA are 0.762, 0.736 and 0.021, respectively, which are also better than that of all the comparison methods. To analyze the capability of DeepUMQA for distinguishing good models from poor models, we use all models in CASP13 and CASP14 datasets to perform a ROC analysis. Figure 3 shows the ROC curves on Global QA and the AUC* (FPR threshold of 0.2) of different nethods sre listed in Supplementary Table S8 in Supplementary Material. In the CASP13 and CASP14 datasets, the AUC of DeepUMQA are 0.940 and 0.886, respectively, which are significantly higher than the value of the comparison methods (ProQ2, ProQ3, ProQ3D, VoroMQA, Ornate, ProteinGCN, ModFOLD7, ModFOLD8, QDeep, ResNetQA, GraphQA and DeepAccNet, respectively). In addition, DeepUMQA also achieved the highest AUC* of 0.780 and 0.581 in the CASP13 and CASP14 datasets, respectively. For Local QA, the performance

Table 1. Comparison of DeepUMQA with other single-model methods on CASP13 dataset

Method	Global QA				Local QA			
	Pear	Spear	Loss	AUC	Pear	Spear	ASE	AUC
DeepUMQA	0.834	0.804	0.046	0.940	0.766	0.740	0.892	0.908
DeepAccNet	0.820	0.797	0.077	0.928	0.740	0.719	0.883	0.902
VoroMQA	0.708	0.690	0.225	0.834	0.550	0.573	0.732	0.809
ModFOLD7	0.848	0.824	0.068	0.910	0.691	0.675	0.814	0.888
ProQ2	0.769	0.743	0.050	0.866	0.653	0.695	0.731	0.890
ProQ3	0.777	0.756	0.240	0.894	0.662	0.696	0.770	0.890
ProQ3D	0.812	0.782	0.086	0.910	0.662	0.689	0.791	0.886
ProteinGCN	0.742	0.726	0.102	0.911	0.505	0.654	0.874	0.876
ResNetQA	0.815	0.778	0.059	0.910	0.704	0.685	0.821	0.855

Note: Pear, Spear, Pearson and Spearman correlation with respect to real lDDT score; Loss: Per-target average 'top 1 loss' with respect to real lDDT score. (The difference between the real lDDT scores of the best model selected from the predicted scores and the actual best model.); AUC, The area under the curve (AUC) of the Receiver operating characteristic (ROC); ASE, Average residue-wise S-score error.

Table 2. Comparison of DeepUMQA with other single-model methods on CASP14 dataset

Method	Global QA				Local QA			
	Pear	Spear	Loss	AUC	Pear	Spear	ASE	AUC
DeepUMQA	0.762	0.736	0.021	0.886	0.680	0.680	0.890	0.849
DeepAccNet	0.753	0.728	0.030	0.878	0.672	0.661	0.874	0.845
ProQ2	0.501	0.477	0.257	0.774	0.470	0.528	0.726	0.745
ModFOLD8	0.731	0.682	0.023	0.846	0.534	0.531	0.802	0.796
GraphQA	0.645	0.627	0.077	0.833	0.596	0.603	0.855	0.817
ProQ3D	0.717	0.687	0.050	0.832	0.520	0.558	0.775	0.787
Ornate	0.696	0.669	0.041	0.856	0.452	0.479	0.775	0.747
QDeep	0.684	0.649	0.154	0.839	0.523	0.556	0.769	0.788
ProteinGCN	0.692	0.664	0.097	0.853	0.422	0.606	0.865	0.812

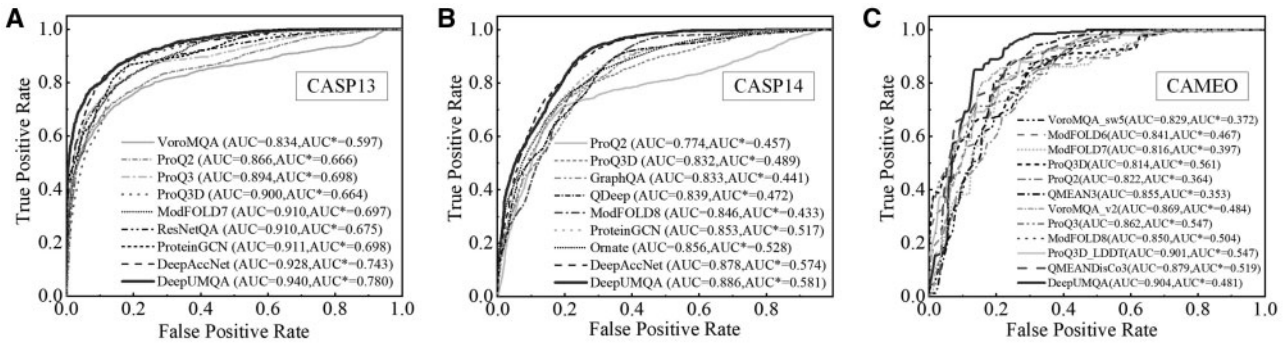

Fig. 3. Receiver operating characteristic (ROC) curve of DeepUMQA and the comparison single-model quality assessment methods on Global QA on the CASP13, CASP14 and CAMEO datasets. An lDDT cutoff value of 0.6 is used to distinguish good and poor models in (**A**) CASP13, (**B**) CASP14 and (**C**) CAMEO datasets, respectively. AUC is the area under the curve of the ROC and AUC* is the partial AUC of the ROC 'trimmed' at a FPR threshold of 0.2, and scaled between 0 and 1. Note that the results of CAMEO come from the 1-month blind test (November 26, 2021 to December 18, 2021)

of DeepUMQA is also excellent. In the CASP13 dataset, DeepUMQA has the highest Pearson (0.766), Spearman correlation (0.740), ASE (0.892) and AUC (0.908), which are 3.51%, 2.92%, 1.02% and 0.67% better than the second-best DeepAccNet, respectively, and the AUC* of DeepUMQA is 0.683, which is second only to ModFOLD7 (0.693). In the CASP14 dataset, in addition to the value of AUC* (0.534) of DeepUMQA, which is second only to DeepAccNet(0.542), other metrics, Pearson (0.680), Spearman correlation (0.680), ASE (0.890) and AUC (0.849) are higher than the second-best DeepAccNet (0.672, 0.661, 0.874 and 0.845, respectively). In CASP13 and CASP14 test datasets, DeepUMQA outperforms the comparison methods in terms of the most metrics.

In order to compare the comprehensive performance of the comparison methods and DeepUMQA, we rank these methods by using the sum of the Z-scores of all metrics on Global QA and Local QA, respectively. Figure 4 shows the ranking of methds in the global and local accuracy estimation. In Figure 4A, B, D and E, it can be easily found that the comprehensive performance of DeepUMQA in the CASP13 and CASP14 datasets is significantly better than the comparison methods, whether in the global or local evaluation.

3.2 Results of CAMEO blind test

Our DeepUMQA server also participated in the blind test of CAMEO-QE (https://www.cameo3d.org/quality-estimation/) for one month (November 26, 2021 to December 18, 2021), and compared the performance with QMEANDisCo3 (Gabriel, 2020), ModFOLD8 (McGuffin *et al.*, 2021), ProQ3 (Uziela *et al.*, 2016) and VoroMQA_sw5, VoroMQA_v2 (Olechnovic and Venclovas, 2017), QMEAN3 (Benkert *et al.*, 2008), ProQ2 (Ray *et al.*, 2012), ProQ3D_LDDT, ProQ3D (Uziela *et al.*, 2017), ModFOLD7 (Maghrabi and McGuffin, 2020) and ModFOLD6 (Maghrabi and McGuffin, 2017).

Table 3 presents the performance of DeepUMQA and the comparison methods in the one-month blind test (November 26, 2021 to December 18, 2021) of CAMEO-QE. And the ROC performance at FPR threshold of 0.2 (AUC*) are listed in Supplementary Tables S8 in Supplementary Material. The results show that for Global QA metrics, DeepUMQA achieves the best Spearman correlation and AUC, which are 0.801 and 0.904, respectively, and the Pearson correlation (0.765) and 'top 1 loss' (0.052) of DeepUMQA are ranked third among all methods. And for Local QA metrics, DeepUMQA has the highest ASE (0.892) compared with the other methods, which are 2.06% better than the second-best ModFOLD8. The Pearson and Spearman correlation of DeepUMQA are 0.761 and 0.743, which are second only to QMEANDisCo3 (0.775 and 0.767, respectively). And the AUC and AUC* of DeepUMQA are 0.894 and 0.660, respectively, which put itself into the top 3 with QMEANDisCo3 and ProQ3D_LDDT. We also rank the methods by using the sum of the Z-scores of Global QA (Fig. 4C) and Local QA (Fig. 4F) metrics to analyze the comprehensive performance of various model quality assessment methods. It can be found that DeepUMQA has the best comprehensive performance in the global evaluation, and its comprehensive performance in local evaluation is second only to QMEANDisCo3, which is better than other comparison methods. The performance of blind test in CAMEO-QE is shown in Supplementary Figures S5–S10 in Supplementary Material.

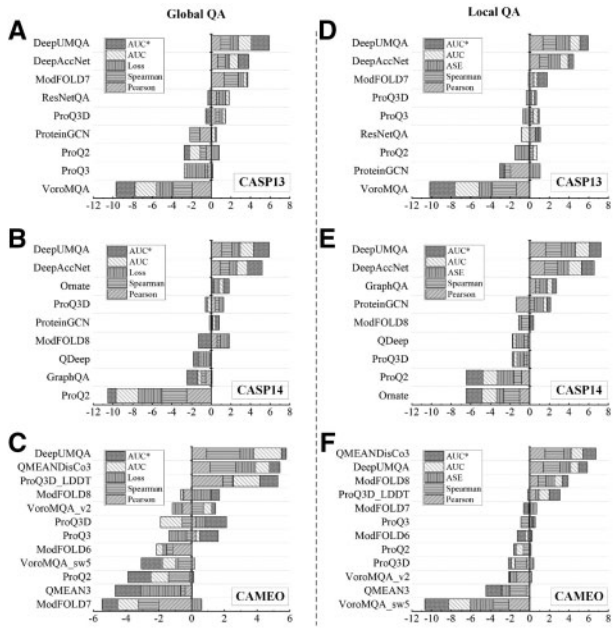

Fig. 4. Ranking of the methods in the global and local accuracy estimation (Global QA and Local QA). (**A**), (**B**) and (**C**) are the sum of Z-scores of the Global QA metrics to rank the methods in the CASP13, CASP14 and CAMEO datasets, respectively. (**D**), (**E**) and (**F**) are the sum of Z-scores of the Local QA metrics to rank the methods in the CASP13, CASP14 and CAMEO datasets, respectively. Note that the results of CAMEO come from the 1-month blind test (November 26, 2021 to December 18, 2021)

3.3 Effect of USR

To verify the effect of the USR feature, we train three comparative versions by using the same dataset and parameters as DeepUMQA, the three versions are DeepUMQA^1 (DeepUMQA without voxelization and USR features), DeepUMQA^2 (DeepUMQA without the voxelization feature) and DeepUMQA^3 (DeepUMQA without the USR feature).

The performance of different versions of DeepUMQA on the CASP13, CASP14 and CAMEO test datasets is shown in Tables 4–6. And the ROC performance at FPR threshold of 0.2 (AUC*) are listed in Supplementary Tables S9 in Supplementary Material. The experimental results show that DeepUMQA^2 with the USR feature has higher Global QA metrics (Pearson, Spearman correlation, 'top 1 loss', AUC and AUC*) compared with DeepUMQA^1 which does not use voxelization and USR features. The Local QA metrics (Pearson, Spearman correlation, ASE, AUC and AUC*) of DeepUMQA^2 are also better than these of DeepUMQA^1. Similarly, the performance of DeepUMQA^3 is improved by the using voxelization feature compared with DeepUMQA^1. Both USR and voxelization features can improve the performance of model quality assessment to some extent, and this result shows that USR and voxelization can both reflect the structural information of residues. Notably, the use of both voxelization and USR features (i.e. DeepUMQA) improves the performance of model quality assessment, and almost all performance indicators are better than those for the three versions on the three test datasets. This result further indicates that USR and voxelization features can complement each

Table 3. Comparison of DeepUMQA with other single-model methods on 1-month CAMEO blind test (November 26, 2021 to December 18, 2021)

Method	Global QA				Local QA			
	Pear	Spear	Loss	AUC	Pear	Spear	ASE	AUC
DeepUMQA	0.765	0.801	0.052	0.904	0.761	0.743	0.892	0.894
QMEANDisCo3	0.773	0.774	0.033	0.879	0.775	0.767	0.856	0.921
ProQ3D_LDDT	0.803	0.720	0.090	0.901	0.690	0.577	0.821	0.901
ModFOLD8	0.711	0.683	0.034	0.850	0.712	0.664	0.874	0.893
ProQ3	0.739	0.669	0.145	0.862	0.632	0.524	0.809	0.874
VoroMQA_v2	0.708	0.727	0.124	0.869	0.528	0.611	0.721	0.871
QMEAN3	0.714	0.673	0.214	0.855	0.610	0.562	0.630	0.851
ProQ2	0.726	0.613	0.087	0.822	0.637	0.540	0.799	0.853
ProQ3D	0.741	0.655	0.066	0.814	0.611	0.493	0.827	0.862
ModFOLD7	0.652	0.619	0.062	0.816	0.646	0.587	0.848	0.871
ModFOLD6	0.685	0.667	0.104	0.841	0.626	0.606	0.798	0.864
VoroMQA_sw5	0.738	0.642	0.101	0.829	0.455	0.458	0.564	0.811

Note: the results of all methods come from the 1-month blind test of CAMEO (November 26, 2021 to December 18, 2021).

Table 4. Performance comparison of different versions of DeepUMQA on the CASP13 dataset

Method	Global QA				Local QA			
	Pear	Spear	Loss	AUC	Pear	Spear	ASE	AUC
DeepUMQA[1]	0.767	0.757	0.118	0.915	0.713	0.704	0.880	0.878
DeepUMQA[2]	0.797	0.774	0.076	0.918	0.728	0.710	0.882	0.885
DeepUMQA[3]	0.819	0.792	0.051	0.928	0.739	0.712	0.881	0.901
DeepUMQA	0.834	0.804	0.046	0.940	0.766	0.740	0.892	0.908

Note: DeepUMQA[1], DeepUMQA without both USR and voxelization features; tem DeepUMQA[2], DeepUMQA without the voxelization feature; DeepUMQA[3], DeepUMQA without the USR feature.

Table 5. Performance comparison of different versions of DeepUMQA on the CASP14 dataset

Method	Global QA				Local QA			
	Pear	Spear	Loss	AUC	Pear	Spear	ASE	AUC
DeepUMQA[1]	0.675	0.665	0.166	0.834	0.590	0.592	0.869	0.797
DeepUMQA[2]	0.708	0.701	0.102	0.849	0.627	0.625	0.879	0.816
DeepUMQA[3]	0.749	0.724	0.053	0.864	0.650	0.645	0.874	0.822
DeepUMQA	0.762	0.736	0.021	0.886	0.680	0.680	0.890	0.849

Table 6. Performance comparison of different versions of DeepUMQA on CAMEO dataset

Method	Global QA				Local QA			
	Pear	Spear	Loss	AUC	Pear	Spear	ASE	AUC
DeepUMQA[1]	0.675	0.665	0.166	0.834	0.590	0.592	0.869	0.797
DeepUMQA[2]	0.708	0.701	0.102	0.849	0.627	0.625	0.879	0.816
DeepUMQA[3]	0.749	0.724	0.053	0.864	0.650	0.645	0.874	0.822
DeepUMQA	0.762	0.736	0.021	0.886	0.680	0.680	0.890	0.849

Note: the results of DeepUMQA come from 1-month blind test (November 26, 2021 to December 18, 2021), and the results of DeepUMQA[1], DeepUMQA[2] and DeepUMQA[3] are obtained locally on the 1-month CAMEO-QE dataset.

other and reflect the topological and local structure information of residues comprehensively. In summary, all of the results emphasize the advantages of using the USR feature for model quality estimation, that is, model quality assessment predictors with the USR feature have better performance in evaluating the global score or the local score of the protein structure.

3.4 Qualitative analysis

Figure 5 shows a quantitative analysis of the quality evaluation of target T1046s2 by using DeepUMQA. Figure 5B shows a comparison of the predicted lDDT and real lDDT for all test models of target T1046s2. They have a strong correlation, especially when the model has high accuracy with lDDT>0.5. The predicted Pearson correlation with the real lDDT is 0.8271, the Spearman correlation is 0.8204, and Kendall's tau correlation is 0.6405. Furthermore, the best model selected based on our predicted lDDT score is consistent with the best model in the actual model pool (the sky-blue dot). Figure 5C shows the ROC curve of all test models of target T1046s2, where AUC is 0.98366, indicating the capability to distinguish good and poor models is excellent. Figure 5D shows the model assessment results of three randomly selected models with different qualities. The first row shows the structure of the three models and their corresponding predicted and real global model qualities, and the second row shows the comparison of the real lDDT (shown in gray) and predicted lDDT (shown in different colors) in each residue. Although differences exist between the predicted lDDT and the real lDDT in several residues, we observe that DeepUMQA can correctly capture the change trend of the lDDT of residue under models with different accuracies, which is important for correcting the mismodeled regions of the model and further model refinement.

4 Conclusion

We developed a USR-based residue-level single-model quality assessment method called DeepUMQA. Residue-level USR and voxelization features, amino acid sequence properties and secondary structure, Rosetta energy terms and distances and orientations extracted from the structure model were used to describe the model information. These features were fed into the deep residual neural network to predict the quality of the protein structure model. The experimental results show that the performance of DeepUMQA in the CASP13 and CASP14 test datasets is better than the state-of-the-art single-model quality assessment methods, including ProQ2, ProQ3, ProQ3D, Ornate, VoroMQA, ProteinGCN, ResNetQA, QDeep, GraphQA, ModFOLD7, ModFOLD8 and DeepAccNet. In addition, the blind test performance of DeepUMQA on CAMEO-QE is at the leading level among the public servers (including QMEANDisCo3, ProQ3D_LDDT, ModFOLD8, ProQ3, VoroMQA_v2, QMEAN3, ProQ2, ProQ3D, ModFOLD7, ModFOLD6 and VoroMQA_sw5). The USR feature describes the residue-level topological structure information, and it is complementary to the voxelization feature that describes the local structure information of the residues. As a result, the residue structure information is comprehensively characterized, and the accuracy of model assessment is considerably improved. With the rapid development of protein structure prediction, the dynamic

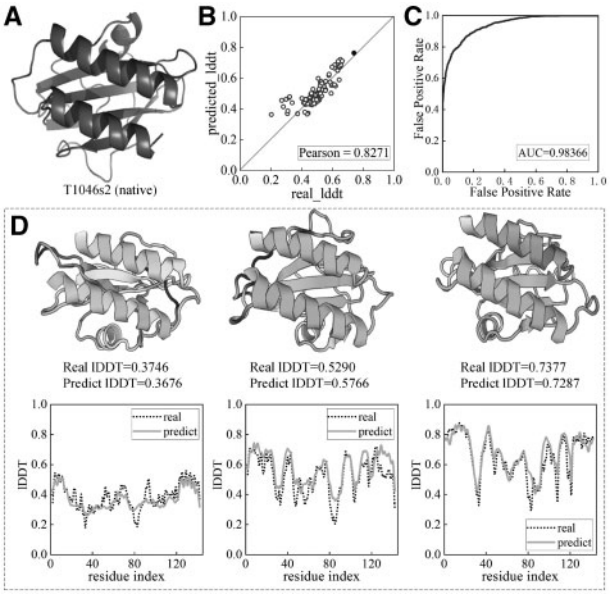

Fig. 5. Qualitative analysis of the performance of DeepUMQA on CASP14 target T1046s2. (**A**) The experimental structure of the target T1046s2. (**B**) Comparison of the predicted lDDT and real lDDT for all test models of target T1046s2 (sky-blue solid point represents the best model). (**C**) The ROC curve of all test models of target T1046s2. (**D**) Results of model assessment of three randomly selected models of target T1046s2 with different quality

combination of model quality assessment and folding process could be a future research direction.

Funding

This work was supported by the 'New Generation Artificial Intelligence' major project of Science and Technology Innovation 2030 of the Ministry of Science and Technology of the People's Republic of China [2021ZD0150100], the National Nature Science Foundation of China [62173304, 61773346] and the Key Project of Zhejiang Provincial Natural Science Foundation of China [LZ20F030002].

Conflict of Interest: none declared.

References

AlQuraishi,M. (2019) AlphaFold at CASP13. *Bioinformatics*, **35**, 4862–4865.
Baldassarre,F. *et al.* (2021) GraphQA: protein model quality assessment using graph convolutional networks. *Bioinformatics*, **37**, 360–366.
Ballester,P.J. and Richards,W.G. (2007) Ultrafast shape recognition to search compound databases for similar molecular shapes. *J. Comput. Chem.*, **28**, 1711–1723.
Benkert,P. *et al.* (2008) QMEAN: a comprehensive scoring function for model quality assessment. *Proteins Struct. Funct. Bioinf.*, **71**, 261–277.
Bolboaca,S.D. *et al.* (2006) Pearson versus Spearman, Kendall's tau correlation analysis on structure-activity relationships of biologic active compounds. *Leonardo J. Sci.*, **5**, 179–200.
Cao,R.Z. *et al.* (2017) QAcon: single model quality assessment using protein structural and contact information with machine learning techniques. *Bioinformatics*, **33**, 586–588.
Cheng,J.L. *et al.* (2009) Prediction of global and local quality of CASP8 models by MULTICOM series. *Proteins Struct. Funct. Bioinf.*, **77**, 181–184.
Cheng,J.L. *et al.* (2019) Estimation of model accuracy in CASP13. *Proteins Struct. Funct. Bioinf.*, **87**, 1361–1377.
Conway,P. *et al.* (2014) Relaxation of backbone bond geometry improves protein energy landscape modeling. *Protein Sci.*, **23**, 47–55.
Gabriel,S. *et al.* (2020) QMEANDisCo—distance constraints applied on model quality estimation. Bioinformatics, **36**, 1765–1771.
Ginalski,K. *et al.* (2003) 3D-Jury: a simple approach to improve protein structure predictions. *Bioinformatics*, **19**, 1015–1018.
Glorot,X. and Bengio,Y. (2010) Understanding the difficulty of training deep feedforward neural networks. In: *Proceedings of the Thirteenth International Conference on Artificial Intelligence and Statistics*, pp. 249–256.
Hao,X.H. *et al.* (2016) A novel method using abstract convex underestimation in ab-initio protein structure prediction for guiding search in conformational feature space. *IEEE/ACM Trans. Comput. Biol. Bioinf.*, **13**, 887–900.
Henikoff,S. and Henikoff,J.G. (1992) Amino acid substitution matrices from protein blocks. *Proc. Natl. Acad. Sci. USA*, **89**, 10915–10919.
Hiranuma,N. *et al.* (2021) Improved protein structure refinement guided by deep learning based accuracy estimation. *Nat. Commun.*, **12**, 11.
Jing,X.Y. and Xu,J.B. (2020) Improved protein model quality assessment by integrating sequential and pairwise features using deep learning. *Bioinformatics*, **36**, 5361–5367.
Jing,X.Y. and Xu,J.B. (2021) Fast and effective protein model refinement using deep graph neural networks. *Nat. Comput. Sci.*, **1**, 462–469.
Jumper,J. *et al.* (2021) Highly accurate protein structure prediction with AlphaFold. *Nature*, **596**, 583–589.
Kabsch,W. and Sander,C. (1983) Dictionary of protein secondary structure: pattern recognition of hydrogen-bonded and geometrical features. *Biopolym. Original Res. Biomol.*, **22**, 2577–2637.
Kingma,D.P. and Ba,J. (2014) Adam: a method for stochastic optimization.*Computer Science*.
Kryshtafovych,A. *et al.* (2018) Assessment of model accuracy estimations in CASP12. *Proteins Struct. Funct. Bioinf.*, **86**, 345–360.
Kryshtafovych,A. *et al.* (2019) Critical assessment of methods of protein structure prediction (CASP)-Round XIII. *Proteins Struct. Funct. Bioinf.*, **87**, 1011–1020.
Kuhlman,B. and Bradley,P. (2019) Advances in protein structure prediction and design. *Nat. Rev. Mol. Cell Biol.*, **20**, 681–697.
Kwon,S. *et al.* (2021) Assessment of protein model structure accuracy estimation in CASP14: old and new challenges. *Proteins Struct. Funct. Bioinf.*, **89**, 1940–1948.
Leaver-Fay,A. *et al.* (2011) ROSETTA3: an object-oriented software suite for the simulation and design of macromolecules. *Methods Enzymol.*, **487**, 545–574.
Li,Y. *et al.* (2021) Deducing high-accuracy protein contact-maps from a triplet of coevolutionary matrices through deep residual convolutional networks. *PLoS Comput. Biol.*, **17**, e1008865.
Ling,C.X. *et al.* (2003) AUC: a statistically consistent and more discriminating measure than accuracy. *IJCAI*, **3**, 519–524.
Liu,J. *et al.* (2020) CGLFold: a contact-assisted de novo protein structure prediction using global exploration and loop perturbation sampling algorithm. *Bioinformatics*, **36**, 2443–2450.
Liu,J. *et al.* (2021) A de novo protein structure prediction by iterative partition sampling, topology adjustment and residue-level distance deviation optimization. *Bioinformatics*, **38**, 99–107.
Lundström,J. *et al.* (2001) Pcons: a neural-network-based consensus predictor that improves fold recognition. *Protein Sci.*, **10**, 2354–2362.
Manavalan,B. *et al.* (2017) SVMQA: support-vector-machine-based protein single-model quality assessment. *Bioinformatics*, **33**, 2496–2503.
Maghrabi,A.H. and McGuffin,L.J. (2017) ModFOLD6: an accurate web server for the global and local quality estimation of 3D protein models. *Nucleic Acids Res.*, **45**, W416–W421.
Maghrabi,A.H. and McGuffin,L.J. (2020) Estimating the quality of 3D protein models using the ModFOLD7 server. *Protein Struct. Prediction*, **2165**, 69–81.
Mao,W. *et al.* (2020) AmoebaContact and GDFold as a pipeline for rapid de novo protein structure prediction. *Nat. Mach. Intell.*, **2**, 25–33.
Mariani,V. *et al.* (2013) lDDT: a local superposition-free score for comparing protein structures and models using distance difference tests. *Bioinformatics*, **29**, 2722–2728.
McGuffin,L.J. *et al.* (2019) IntFOLD: an integrated web resource for high performance protein structure and function prediction. *Nucleic Acids Res.*, **47**, W408–W413.
McGuffin,L.J. *et al.* (2021) ModFOLD8: accurate global and local quality estimates for 3D protein models. *Nucleic Acids Res.*, **49**, W425–W430.
Meiler,J. *et al.* (2001) Generation and evaluation of dimension-reduced amino acid parameter representations by artificial neural networks. *Mol. Model. Annu.*, **7**, 360–369.
Metz,C.E. (1978) Basic principles of ROC analysis. *Semin. Nuclear Med.*, **8**, 283–298.
Moult,J. *et al.* (2018) Critical assessment of methods of protein structure prediction (CASP)-Round XII. *Proteins Struct. Funct. Bioinf.*, **86**, 7–15.
Olechnovic,K. and Venclovas,C. (2017) VoroMQA: assessment of protein structure quality using interatomic contact areas. *Proteins Struct. Funct. Bioinf.*, **85**, 1131–1145.

Pagès,G. *et al.* (2019) Protein model quality assessment using 3D oriented convolutional neural networks. *Bioinformatics*, **35**, 3313–3319.
Ray,A. *et al.* (2012) Improved model quality assessment using ProQ2. *BMC Bioinformatics*, **13**, 1–12.
Rohl,C.A. *et al.* (2004) Protein structure prediction using Rosetta. *Methods Enzymol.*, **383**, 66–93.
Sanyal,J. *et al.* (2020) ProteinGCN: protein model quality assessment using graph convolutional networks. *bioRxiv*, doi: 10.1101/2020.04.06.028266.
Senior,A.W. *et al.* (2020) Improved protein structure prediction using potentials from deep learning. *Nature*, **577**, 706–710.
Shuvo,M.H. *et al.* (2020) QDeep: distance-based protein model quality estimation by residue-level ensemble error classifications using stacked deep residual neural networks. *Bioinformatics*, **36**, i285–i291.
Song,Y. *et al.* (2013) High-resolution comparative modeling with RosettaCM. *Structure*, **21**, 1735–1742.
Uziela,K. *et al.* (2016) ProQ3: improved model quality assessments using Rosetta energy terms. *Sci. Rep.*, **6**, 1–10.
Uziela,K. *et al.* (2017) ProQ3D: improved model quality assessments using deep learning. *Bioinformatics*, **33**, 1578–1580.
Wang,G.L. *et al.* (2003) PISCES: a protein sequence culling server. *Bioinformatics*, **19**, 1589–1591.
Wang,S. *et al.* (2017) Accurate de novo prediction of protein contact map by ultra-deep learning model. *PLoS Comput. Biol.*, **13**, e1005324.
Won,J. *et al.* (2019) Assessment of protein model structure accuracy estimation in CASP13: challenges in the era of deep learning. *Proteins Struct. Funct. Bioinf.*, **87**, 1351–1360.
Xu,D. and Zhang,Y. (2012) Ab initio protein structure assembly using continuous structure fragments and optimized knowledge-based force field. *Proteins Struct. Funct. Bioinf.*, **80**, 1715–1735.
Xu,J.B. and Wang,S. (2019) Analysis of distance-based protein structure prediction by deep learning in CASP13. *Proteins Struct. Funct. Bioinf.*, **87**, 1069–1081.
Xu,J.B. (2019) Distance-based protein folding powered by deep learning. *Proc. Natl. Acad. Sci. USA*, **116**, 16856–16865.
Yang,J.Y. *et al.* (2015) The I-TASSER Suite: protein structure and function prediction. *Nat. Methods*, **12**, 7–8.
Yang,J.Y. *et al.* (2020) Improved protein structure prediction using predicted interresidue orientations. *Proc. Natl. Acad. Sci. USA*, **117**, 1496–1503.
Zhang,G.J. *et al.* (2017) Enhancing protein conformational space sampling using distance profile-guided differential evolution. *IEEE/ACM Trans. Comput. Biol. Bioinf.*, **14**, 1288–1301.
Zheng,W. *et al.* (2021) Folding non-homologous proteins by coupling deep-learning contact maps with I-TASSER assembly simulations. *Cell Rep. Methods*, **1**, 100014.
Zhou,X.G. *et al.* (2019a) Assembling multidomain protein structures through analogous global structural alignments. *Proc. Natl. Acad. Sci. USA*, **116**, 15930–15938.
Zhou,X.G. *et al.* (2019b) Underestimation-assisted global-local cooperative differential evolution and the application to protein structure prediction. *IEEE Trans. Evol. Comput.*, **24**, 536–550.
Zhou,X.G. *et al.* (2020) Progressive and accurate assembly of multi-domain protein structures from cryo-EM density maps. *bioRxiv*, doi: 10.1101/2020.10.15.340455.